

Response of an artificially blown clarinet to different blowing pressure profiles.

B. BERGEOT^{a,*}, A. ALMEIDA^a, C. VERGEZ^b, B. GAZENGEL^a, D. FERRAND^c

^aLUNAM Université, Université du Maine, UMR CNRS 6613, Laboratoire d'Acoustique, Avenue Olivier Messiaen, 72085 Le Mans Cedex 9, France

^bLaboratoire de Mécanique et Acoustique (LMA, CNRS UPR7051), 31 Chemin Joseph Aiguier, 13402 Marseille Cedex 20, France

^cLaboratoire d'Astrophysique de Marseille (LAM-CNRS-INSU UMR 7326), Pôle de l'Étoile Site de Château-Gombert / 38, rue Frédéric Joliot-Curie 13388 Marseille Cedex 13, France

Abstract

Using an artificial mouth with an accurate pressure control, the onset of the pressure oscillations inside the mouthpiece of a simplified clarinet is studied experimentally. Two time profiles are used for the blowing pressure: in a first set of experiments the pressure is increased at constant rates, then decreased at the same rate. In a second set of experiments the pressure rises at a constant rate and is then kept constant for an arbitrary period of time. In both cases the experiments are repeated for different increase rates.

Numerical simulations using a simplified clarinet model blown with a constantly increasing mouth pressure are compared to the oscillating pressure obtained inside the mouthpiece. Both show that the beginning of the oscillations appears at a higher pressure values than the theoretical static threshold pressure, a manifestation of bifurcation delay.

Experiments performed using an interrupted increase in mouth pressure show that the beginning of the oscillation occurs close to the stop in the increase of the pressure. Experimental results also highlight that the speed of the onset transient of the sound is roughly the same, independently of the duration of the increase phase of the blowing pressure.

Keywords: Musical acoustics, Clarinet-like instruments, Transient processes, Iterated maps, Dynamic Bifurcation, Bifurcation delay.

1. Introduction

The clarinet is one of the most well-described instrument in terms of scientific theories for its behavior. The relative simplicity of its elements and their couplings has allowed to explain several features of the sustained sound of the clarinet, such as the playing frequency, the harmonic content, or the amplitude of the sound, and their variation with the action of the musician on its instrument. An important part of the timbre of this musical instrument can thus be understood with currently existing models. However, the timbre does not only depend on the characteristics of the sustained sound but to a great extent, on the quick variations that happen at the onset of the sound, i. e., the attack transient.

The first studies [1, 2, 3, 4, 5, 6] concerning the clarinet assume that the mouth pressure is constant and does not depend on time. We call this approach the “static case”. These studies use simple resonator models (single mode [1], iterated map[2, 3] or continuation methods of the Hopf bifurcation[7]) and a linear approximation of the non-linear characteristic function of the exciter to predict the threshold pressure, the bifurcation diagram and the temporal shape of the pressure inside the mouthpiece. Results show that the oscillation threshold pres-

sure, which will be called in this article the “static oscillation threshold” is related to reed stiffness, the mouthpiece opening and the losses inside the resonator [4, 2]. The calculated and the measured thresholds show qualitative agreement if the threshold pressure is measured while the mouth pressure is slowly decreasing [5]. Prediction of the transient using a linearization of the exciter characteristic agrees well with numerical simulations [1] and shows that the acoustic pressure starts with an exponential envelope before reaching saturation [6]. For a given resonator and a fixed embouchure, the γ coefficient of the exponential growth ($p_0 e^{\gamma t}$) depends only on the value of the constant mouth pressure.

In a real situation, the attack of a note is produced with a complex combined action of several gestures. In special occasions, a musician will perform a “breath attack” without using his tongue. These transients show that the mouth pressure increases quickly, typically in 40ms [8] and that players overshoot a desired blowing pressure and then “decay” back to a “sustain” level.

More recent articles have studied the behavior of the instrument for time-varying pressures. Typically, these have used “Continuous Increasing Mouth Pressure” (CIMP), in which the blowing pressure increases with time at a constant rate, and “Interrupted Increasing Mouth Pressure followed by a Plateau” (IIMPP), in which the constant

*Corresponding author, baptiste.bergeot@univ-lemans.fr

increase is stopped at the “interrupting time”, being followed by a constant pressure. Using a CIMP, Atig *et al* [9] notices that oscillation threshold pressure calculated using numerical simulation is higher than the static oscillation threshold. Bergeot *et al* [10] provide an analytical/numerical study of a simple clarinet model (also used in this paper and presented in section 3) in CIMP situations and propose the term “dynamic oscillation threshold” to define the beginning of mouthpiece pressure oscillation in dynamic cases. An analytical expression is proposed for the dynamic threshold, predicting that it is always higher than the “static threshold”. This phenomenon is known in mathematical literature as *bifurcation delay* [11]. We wish to emphasize that the term “delay” in *bifurcation delay* does not necessarily refer to a time difference but to a shift in the oscillation threshold. In this work, the word “delay” often refers to that shift.

The comparison between theoretical results and numerical simulations reveals an important sensitivity to the precision (i.e. the number of digits) used in numerical simulations. Indeed, numerical results only converge to the theory when the simplified model (the same as used for analytical investigation) is computed with hundreds or thousands of digits [10]. Otherwise, theoretical results become useless in predicting the behavior of the simulated model. In this case, the dynamic threshold increases with the increase rate of the mouth pressure. Silva [12] performs numerical simulations of an IIMPP, showing that the beginning of the envelope of the mouthpiece pressure is an exponential $p_0 e^{\gamma t}$ arising once the mouth pressure stops increasing, and in which the growth constant γ does not depend on the duration of the mouth pressure increase.

In this paper, the operation of a simplified clarinet under simplified conditions (CIMP and IIMPP mouth pressure profiles) is studied experimentally. The “clarinet” is a simple cylindrical tube attached to a clarinet mouthpiece – it has no bore variations, no flare, no bell and no tone or register holes.

To characterise the onset, three main parameters will be used: the time (or value of mouth pressure) at the start of the oscillations, their initial amplitude, and the growth constant (which as will be seen, can vary through time in some cases). These parameters can be equivalently expressed as a function of time or as a function of mouth pressure, since the latter is an affine function of time.

In the case of the CIMP profile, these parameters, measured using the artificial mouth, are compared to the parameters estimated using simulations of a simplified clarinet model for different values of the increase rate of the CIMP.

In the case of the IIMPP, the starting time of the oscillations and the growth constant are related to the characteristics of the mouth pressure profile, in particular the “interrupting time” of the IIMPP, and the value of constant pressure reached at the end of the IIMPP.

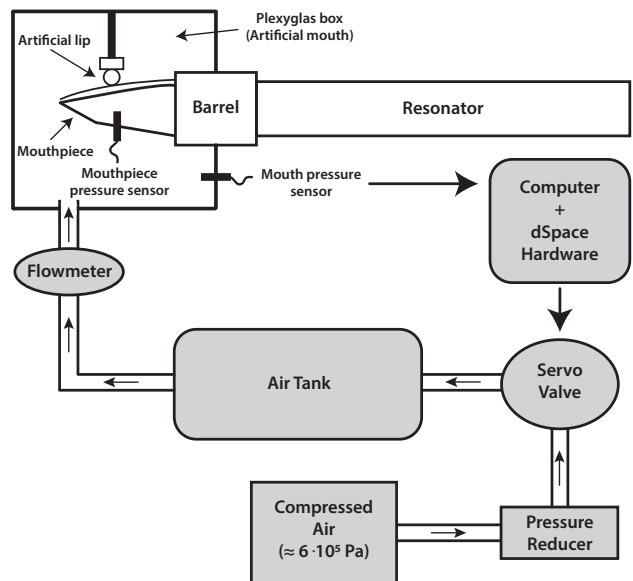


Figure 1: Principle of the Pressure Controlled Artificial Mouth (PCAM).

The paper is organized as follows: section 2 presents the experimental system (artificial mouth). Section 3 presents the physical model used for simulating the clarinet system. The experimental results are presented and discussed in section 4 for CIMP profiles and in section 5 for IIMPP profiles of mouth pressure. In section 4 experimental results obtained for CIMP profiles are compared to numerical simulations.

2. Experimental setup and configurations

We describe here the experimental setup and the two experimental protocols used in the work. An outline schematic of the experimental setup is presented in fig. 1.

2.1 Materials

A simplified clarinet is inserted by its mouthpiece into Pressure Controlled Artificial Mouth (PCAM). The PCAM is responsible for controlling the mouth pressure and provides a suitable support for the sensors used in measuring the physical quantities of interest [13, 14].

The simplified clarinet is made of a plastic cylinder connected to the barrel of a real clarinet. The total length of cylinder and barrel is $l = 0.52\text{m}$ (this is also the effective length of the instrument, calculated from $L = c/4f$, where c is the sound velocity and f the playing frequency) and the internal diameter is 15mm.

The artificial mouth is made of a Plexiglas box which supports rigidly both the mouthpiece and the barrel. It is a chamber with an internal volume of 30cm^3 where the air pressure P_m is to be controlled. The artificial lip is made of a foam pad sitting on the reed.

Both the internal mouth pressure and the pressure inside the mouthpiece are measured using differential pressure sensors (*Endevco 8510B* and *8507C* respectively). Finally, a flowmeter (*Bürkert 870I*) is placed at the entrance of the artificial mouth to measure the input volume flow entering into the reed channel.

Control of the mouth pressure is based on high-precision regulation of the air pressure inside the Plexiglas box. This regulation enables the control of blowing pressure around a target which can either be a fixed value or follow a function varying slowly over time. A servo-valve (*Bürkert 2832*) is connected to a compressed air source through a pressure reducing valve. The servo valve is a proportional valve in which the opening is proportional to the electric current. The maximum pressure available is approximately $6 \cdot 10^5 \text{Pa}$. A pressure reducer is used to adjust the pressure upstream the servo-valve which is connected to the entrance of the artificial mouth itself. An air tank (120 litres) is inserted between of the servo-valve and the artificial mouth in order to stabilize the feedback loop during slowly varying onsets. This large tank is used for experiments performed with the CIMP profile, and is replaced by a much smaller tank (approx. 2 litres) when faster varying targets are tested (IIMPP profile). The control algorithm is implemented on a DSP card (*dSpace DS1104*), modifying the volume flow through the servo-valve every $40 \mu\text{s}$ in order to minimize the difference between the measured and the target mouth pressure. Moreover, because of the long response time of the flowmeter, the volume flow is measured but is not used in the control loop.

2.2 Experimental protocol

2.2.1 "CIMP" profile

Starting from a low value (0.2 kPa in our experiment) the mouth pressure $P_m(t)$ is increased at a constant rate k (the slope) until a few seconds after the clarinet starts to sound. The mouth pressure is then decreased with a symmetric slope ($k' = -k$). During the experiment, the mouth pressure $P_m(t)$, the pressure in the mouthpiece $P(t)$ and the incoming flow $U(t)$ are recorded. Fig. 2 shows an example of the time profile of P_m and P with $k = 0.1 \text{ kPa/s}$.

The experiment is repeated three times for each of the target slope values k given as a command to the PCAM. The actual values of the slope obtained during the experiment are estimated using a linear fit and shown in table 1. We can see that the use of the PCAM provides a very good repeatability on the increase/decrease rate of the blowing pressure.

2.2.2 "IIMPP" profile

For the IIMPP profile, the blowing pressure has two phases, first increasing at a faster rate than that used for the CIMP profile, then kept at an almost constant value.

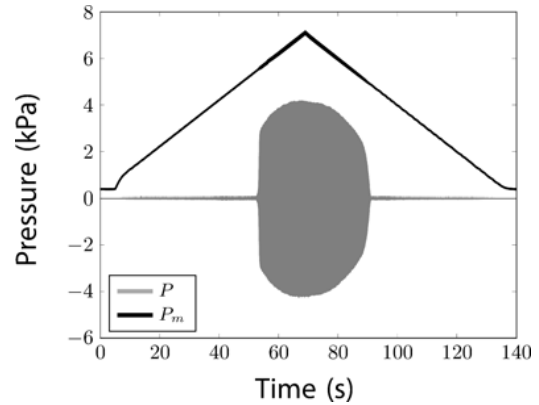


Figure 2: Time evolution of the mouth pressure $P_m(t)$ (CIMP profile) and of the pressure inside the mouthpiece $P(t)$. The slope k of the mouth pressure is equal to 0.1 kPa/s .

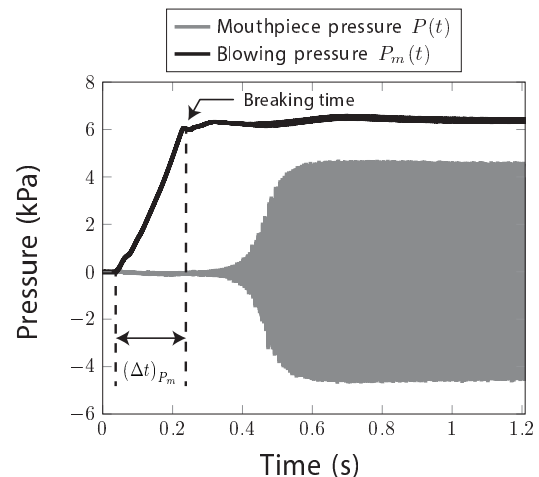


Figure 3: Measured signals in an IIMPP case: blowing pressure $P_m(t)$ (solid black line) and pressure inside the mouthpiece $P(t)$ (solid gray line).

Table 1: Estimation of the slope for each repetition in experiment plus averages.

Experiment	1	2	3	4	5	6
Values of k (kPa/s) (incr. blowing pressure)						
1 st time	0.100	0.140	0.233	0.751	1.557	2.681
2 nd time	0.100	0.140	0.233	0.752	1.557	2.712
3 rd time	0.100	0.140	0.233	0.753	1.559	2.711
Average	0.100	0.140	0.233	0.752	1.558	2.702

For example, in fig. 3, the blowing pressure P_m starts at a low value (approx. 0.1 kPa), increases for a certain time (hereafter referred as $(\Delta t)_{P_m}$), reaches a target value (approx. 7 kPa) and is then kept constant. The experiment is repeated for different values of $(\Delta t)_{P_m}$ (target values are 0.05s, 0.2s, 0.5s and 1s corresponding respectively to experiments numbered 1, 2, 3 and 4, cf. table 2) and repeated fifteen times for each value of $(\Delta t)_{P_m}$. Table 2 shows a good agreement between the command and the measurement of $(\Delta t)_{P_m}$. This indicates that the control of the PCAM works even for rapid variations in blowing pressure. However, for the fastest (experiment 1), the difference between the command and measurement is about 50% of the command. Table 2 also shows good repeatability of the blowing pressure slope during the increasing part.

In this experiment, only the blowing pressure P_m and the internal mouthpiece pressure P are recorded (see fig. 3).

3. Clarinet model

This section presents the physical model of the clarinet used in this work. The numerical simulations of the model will be compared to experimental results in section 4 for the CIMP profile.

3.1 Equations

The model divides the instrument into two elements, the exciter and the resonator.

3.1.1 Exciter

The exciter of a clarinet is the reed-mouthpiece system, characterized by four physical quantities, the flow U across the reed channel, the pressure difference $\Delta P = P_m - P$, the reed position y and the reed volume velocity U_r (fig. 4). For lower frequencies than the resonance frequency of the reed, and in a non-beating regime (this is the case in this work because we study the beginning of the oscillations), U_r can be considered as a length correction [15]. We thus assume that $U_r = 0$ so that $U = U_{in}$, and take the length correction into account in the effective length of the resonator. Ignoring reed damping and inertia, the pressure difference and reed position are proportional.

With these assumptions, the model can be described by two physical quantities ΔP and U linked through the nonlinear characteristics of the exciter:

$$\begin{cases} U = \frac{\zeta}{Z_c} (P_M - \Delta P) \sqrt{\frac{|\Delta P|}{P_M}} \operatorname{sgn}(\Delta P), & (1a) \\ 0, & \text{if } \Delta P < P_M ; \\ 0, & \text{if } \Delta P > P_M, \end{cases} \quad (1b)$$

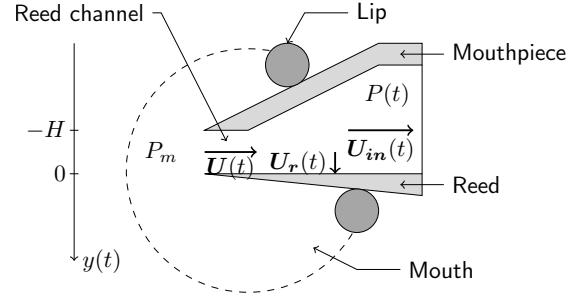


Figure 4: View of the physical quantities used in the model.

where P_M is the static closing pressure of the reed. Parameter ζ is a non dimensional parameter written as

$$\zeta = Z_c S \sqrt{\frac{2}{\rho P_M}}, \quad (2)$$

where S is the cross-section of the reed channel at rest, ρ the air density and $Z_c = \rho c / S_{cyl}$ the characteristic impedance of the cylindrical resonator of cross-section S_{cyl} .

3.1.2 Resonator

The resonator is assumed to be a perfect cylinder in which only plane waves propagate. In linear acoustics, any unidimensional single-frequency pressure distribution can be expanded into two waves propagating in opposite directions. Using this property, the acoustic pressure P is the sum of an outgoing wave P^+ and an incoming wave P^- :

$$P^+ = \frac{1}{2} (P + Z_c U) \quad ; \quad P^- = \frac{1}{2} (P - Z_c U). \quad (3)$$

Using the variables P^+ and P^- instead of the variables P and U , the resonator can be described by its reflection function $r(t)$, satisfying

$$P^-(t) = (r * P^+)(t). \quad (4)$$

A monochromatic planar wave of frequency f propagates in the resonator with a damping factor α taking into account the visco-thermal losses, which at low frequencies are dominant over the radiation losses. The approximate expression of α is [16]:

$$\alpha \approx 3 \cdot 10^{-5} \sqrt{f/R}, \quad (5)$$

where R is the bore radius.

Even if the acoustic signals P^+ and P^- are not monochromatic, the damping factor α is assumed to be constant, calculated at the playing frequency [17, 18, 19, 20, 2] and ignoring dispersion. Using this restrictive assumption Dalmont and Frappe [5] obtain a good agreement between theoretical and experimental results for threshold, in particular the oscillation threshold, provided

Table 2: Averages and standard deviations of the measured $(\Delta t)_{P_m}$ and k obtained for each PCAM command for $(\Delta t)_{P_m}$.

Experiment	1	2	3	4
Command for $(\Delta t)_{P_m}$ (s)	0.05	0.2	0.5	1
Average of measured $(\Delta t)_{P_m}$: $\overline{(\Delta t)_{P_m}}$ (s)	0.0747	0.2047	0.4590	0.9168
Standard deviation of measured $(\Delta t)_{P_m}$ (s)	0.0100	0.0108	0.0029	0.0060
Average of measured k : \bar{k} (kPa/s)	80.7354	29.9284	13.4157	7.4133
Standard deviation of measured k (kPa/s)	7.6354	1.0262	0.2061	0.0378

that embouchure parameters P_m and ζ are well estimated. Because the damping factor α is assumed to be constant, the reflection function $r(t)$ becomes a simple delay with sign inversion (multiplied by an attenuation coefficient λ) and is written

$$r(t) = -\lambda\delta(t - \tau), \quad (6)$$

where,

$$\lambda = e^{-2\alpha L}, \quad (7)$$

is the attenuation coefficient, $\tau = 2L/c$ is the travel time of the wave over the resonator length L at speed c .

3.2 Solutions

From equation (6), equation (4) can be simplified as follows:

$$P^-(t) = -\lambda P^+(t - \tau). \quad (8)$$

Moreover, by substituting the variables P and U with variables P^+ and P^- in equation (1) we have:

$$P^+ = G(-P^-). \quad (9)$$

An explicit expression for function G can be found in Taillard *et al* [3], recalled in appendix A and plotted in fig. 5.

Using equations (8) and (9), the complete system can be described by the following equation:

$$P^+(t) = G(\lambda P^+(t - \tau)). \quad (10)$$

Finally, knowing variables P^+ and P^- , it is possible to calculate P using

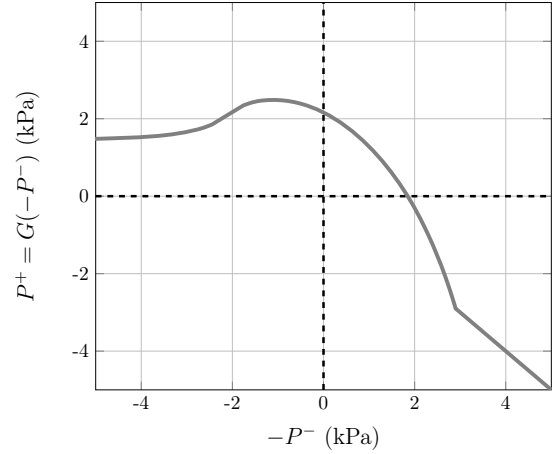
$$P(t) = P^+(t) + P^-(t) = P^+(t) - \lambda P^+(t - \tau), \quad (11)$$

and U using

$$Z_c U(t) = P^+(t) - P^-(t) = P^+(t) + \lambda P^+(t - \tau). \quad (12)$$

3.3 Static oscillation threshold

A study of the stability of the fixed points of function G based on the usual static bifurcation theory (i.e. assuming

**Figure 5:** Function G for $\zeta = 0.6$, $P_M = 10\text{kPa}$ and $Z_c = 3.6 \cdot 10^4 \text{ kPa} \cdot \text{s} \cdot \text{m}^{-3}$.

that the mouth pressure is constant over time) gives an analytical expression P_{mst} of the static oscillation threshold [4]:

$$P_{mst} = \frac{1}{9} \left(\frac{\tanh(\alpha l)}{\zeta} + \sqrt{3 + \left(\frac{\tanh(\alpha l)}{\zeta} \right)^2} \right)^2 P_M. \quad (13)$$

In practice P_{mst} is the minimum value of a static blowing pressure above which an instability can emerge.

Using a linearization of the characteristic curve of the exciter, it can be shown [6] that if the mouth pressure P_m is constant and lower than P_{mst} , the mouthpiece pressure $P(t)$ converges exponentially to a non oscillating regime (called *static regime* in the literature). If P_m is higher than P_{mst} , the pressure $P(t)$ increases exponentially from the *static regime* reaching asymptotically a signal of constant amplitude. For a given resonator and a fixed embouchure (i.e. a given ζ in the model), the time growth constant γ of the exponential depends only on the value of the constant mouth pressure.

4. Results for the "CIMP" profile

The aim of this section is to compare the parameters of the transient deduced from experimental signals and numerical signals. The parameters of interest are:

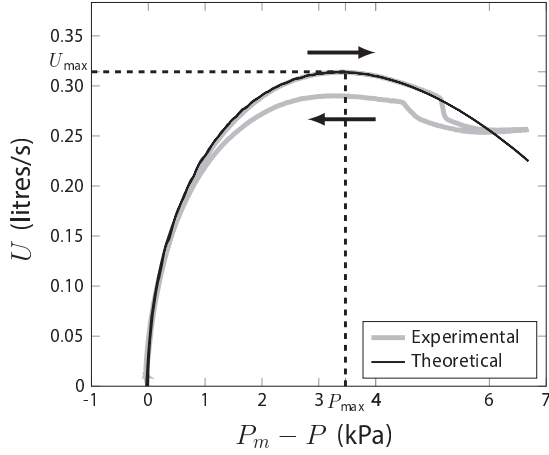


Figure 6: Experimental nonlinear characteristics of the exciter (gray line) for increasing and decreasing blowing pressure and comparison with fitted model (black line) for increasing blowing pressure. ($\zeta = 0.19$ and $P_M = 10.12$ kPa) In this example the increase rate k of the blowing pressure is equal to 0.1 kPa/s.

- The *bifurcation delay* BD defined as the difference between the *dynamic oscillation threshold* P_{mdt} and the analytical *static oscillation threshold* P_{mst} defined through equation (13).
- The time growth constant τ of the onset transient of the RMS envelope of $P(t)$.
- The pressure growth constant η of the onset transient of the RMS envelope of $P(P_m)$.

Firstly, the input parameters of the theoretical model (ζ and P_M) are estimated from the experimental data in order to calculate the value of P_{mst} and to calculate the values of P deduced from equations (10) and (11). Secondly, the method used for calculating the parameters BD , τ and η is presented, as shown in fig. 7.

Then, the method is applied to experimental and numerical signals leading to experimental parameters BD^{exp} , τ^{exp} and η^{exp} and to numerical parameters BD^{num} , τ^{num} and η^{num} . Finally, we compare transient parameters deduced from experimental and simulated signals.

4.1 Estimation of the parameters used in the model

The damping factor α is calculated at the playing frequency, which is around 160Hz, using equation (5). Parameters P_M and ζ are deduced from the experimental non linear characteristics of the exciter, prior to the oscillation, by estimating the coordinates of the maximum of the characteristic curve (P_{max} , U_{max}), through equations (14) and (15):

$$P_{max} = \frac{P_M}{3}, \quad (14)$$

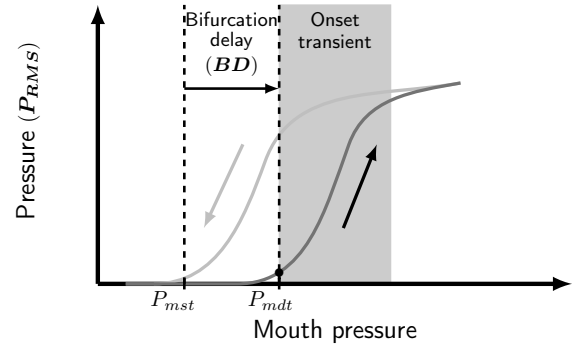
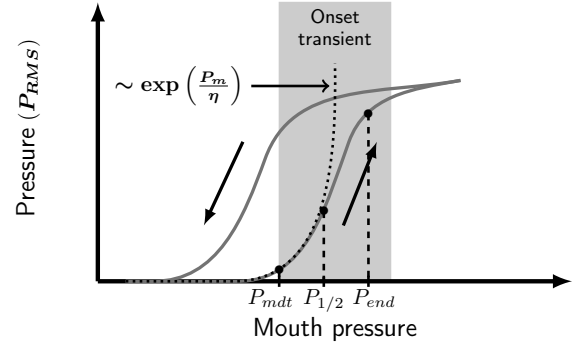
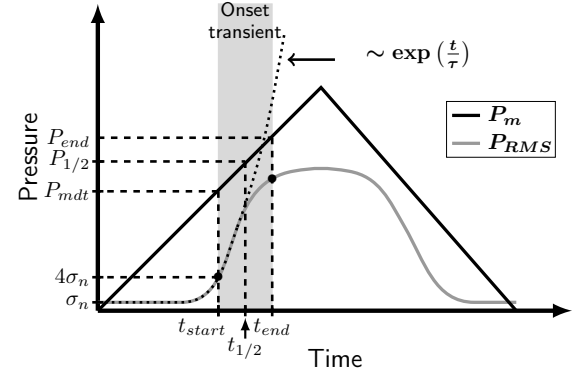


Figure 7: Outline schematic showing the definition of the different indicators of the transient. At the top: blowing pressure P_m and of the RMS envelope P_{RMS} of the pressure inside the mouthpiece as functions of time. Illustrations of t_{start} , t_{end} , P_{mdt} , P_{end} and τ . In the middle: P_{RMS} as a function of P_m . Illustration of η . At the bottom: illustration of the bifurcation delay (BD), corresponding to the pressure difference between the dynamic oscillation threshold P_{mdt} and the static oscillation threshold P_{mst} (see equation (16)).

Table 3: Averages of the slope k , of the parameters P_M , ζ and of the static oscillation threshold P_{mst} obtained for increasing and decreasing blowing pressure.

Experiment	1	2	3	4	5	6
Increasing blowing pressure						
k (kPa/s)	0.100	0.140	0.233	0.752	1.558	2.702
P_M (kPa)	10.1249	10.1018	10.3133	10.6686	11.3559	11.7668
ζ (Ad.)	0.1858	0.1858	0.1829	0.1755	0.1619	0.1614
P_{mst} (kPa)	3.9811	3.9723	4.0658	4.2358	4.5760	4.7448
Decreasing blowing pressure						
k' (kPa/s)	-0.100	-0.140	-0.235	-0.707	-0.679	-0.631
P_M (kPa)	10.0302	9.8651	9.9945	10.2835	10.4859	10.4577
ζ (Ad.)	0.1734	0.1763	0.1750	0.1685	0.1616	0.1646
P_{mst} (kPa)	3.9806	3.9040	3.9602	4.1018	4.2155	4.1903

and

$$U_{\max} = \frac{2}{3\sqrt{3}} \frac{P_M}{Z_c} \zeta. \quad (15)$$

Figure 6 shows an example of an experimental nonlinear characteristic (gray line). As stated previously [21, 22, 5], due to the visco-elasticity of the reed, there is a difference between the characteristics measured for increasing and decreasing blowing pressures.

The values of the parameters ζ and P_M estimated for the 6 values of the slope k (table 1) are given in table 3 for the increasing and decreasing blowing pressures. The difference between the parameters estimated in both cases is low (less than 2 %). For this reason, we used the values of ζ and P_M deduced for increasing blowing pressure. In this case, the value of the static oscillation threshold pressure is calculated using the first three values of k and leads to $P_{mst} = 4.01$ kPa. Due to the response time of the flowmeter (≈ 0.3 s), in experiments 4, 5 and 6 (with faster varying pressures) the closing pressure P_M and static oscillation threshold P_{mst} are overestimated.

4.2 Estimation method of bifurcation delay and growth constants

As a reminder, due to the affine relation between pressure and time, the difference in time, between the time at which the mouth pressure crosses the static threshold and the moment the oscillations actually start can be mapped to a pressure difference. The bifurcation delay BD is formally defined as the difference in threshold values of the mouthpieces pressure:

$$BD = P_{mdt} - P_{mst}, \quad (16)$$

with P_{mdt} the dynamic oscillation threshold and P_{mst} the static oscillation threshold estimated in the previous section (see fig. 7, at the bottom). P_{mdt} is estimated as follows: considering that the acoustic pressure P is a zero mean signal with variance σ_n^2 before the threshold, the beginning of the oscillation, at time t_{start} , is empirically estimated when $P_{RMS}(t_{start}) \geq 4\sigma_n$. Then the dynamic oscillation threshold is defined as $P_{mdt} = P_m(t_{start})$ (cf.

fig. 7).

The part of the signal used for the determination of σ_n is manually delimited. The mean value of the standard deviation of the noise σ_n over all the measurements is 0.01kPa ($\approx 0.35\%$ of the P_{RMS} value during the stationary regime).

For the estimation of the growth constants τ and η , firstly the end time of the transient t_{end} is estimated as the time corresponding to a local minimum of the second derivative of the RMS envelope [23]. Then, assuming that the transient is exponential for a time-varying mouth pressure as it is for linear looped systems in static case, the time growth constant τ is calculated between t_{start} and $t_{1/2} = t_{start} + (t_{end} - t_{start})/2$, as follows:

$$\tau = \frac{t_{1/2} - t_{start}}{\ln(P_{RMS}(t_{1/2})) - \ln(P_{RMS}(t_{start}))}. \quad (17)$$

Given that the blowing pressure is an affine function of time, P_{RMS} can be described using similar functions of either time or blowing pressure. The growth constant η is therefore calculated on $P_{RMS}(P_m)$ between $P_{mdt} = P_m(t_{start})$ and $P_{1/2} = P_m(t_{1/2})$:

$$\eta = \frac{P_{1/2} - P_{mdt}}{\ln(P_{RMS}(t_{1/2})) - \ln(P_{RMS}(t_{start}))}. \quad (18)$$

4.3 Comparison between experiment and simulation

Experimental signals are first compared to numerical solutions of equations (10) and (11). The simulation uses the experimental blowing pressure $P_m(t)$ and reed parameters ζ and P_M estimated in section 4.1. Then, experimental parameters BD^{exp} , τ^{exp} and η^{exp} are compared to numerical parameters BD^{num} , τ^{num} and η^{num} .

4.3.1 Comparison between experimental and numerical pressure signals

In fig. 8, the RMS envelope P_{RMS} is plotted as a function of the mouth pressure P_m for different slopes of the blowing pressure (fig. 8(a): experimental signals and fig. 8(b): simulated signals). First of all, in fig. 8(a), it is worth noting that for all values of the slope k , the state reached

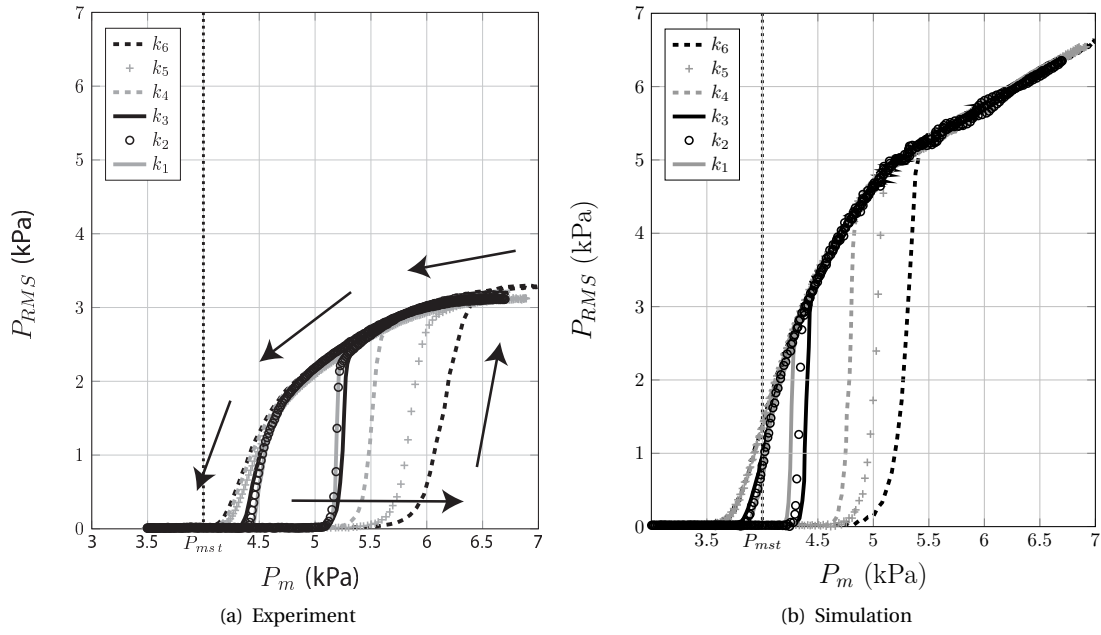


Figure 8: P_{RMS} plotted against P_m for each value of the slope k . (a) Experimental signals, (b) signals generated by the numerical simulation of the model with parameters ζ and P_M estimated experimentally (cf. section 4.1), plotted against the measured blowing pressure $P_m(t)$. Arrows represent the evolution through time and highlight an hysteresis cycle.

at the end of the transient belongs to the same periodic branch (slight repeatability errors aside).

Secondly, we can observe a substantial difference between the experimental and numerical signal amplitudes. Two reasons can explain this difference. The first is the fact that the damping factor is estimated at the playing frequency. A second reason could be the error made on the estimation of the reed parameters. Note also that the model used for these simulations is a very rough approximation to the instrument under study.

Figure 8 highlights a hysteresis cycle: the dynamic threshold estimated during the increasing phase is higher than the value of P_m at which oscillation stops during the decreasing phase. Figure 6 shows a change of embouchure parameters between the ascending and descending phases of the blowing pressure. Although this could explain the hysteresis cycle observed in fig. 8(a) (experimental results), the hypothesis is not confirmed by numerical results shown in fig. 8(b). Indeed, numerical simulations are run with constant embouchure parameters during the ascending and descending phases of the blowing pressure, also showing a hysteresis cycle. This provides a strong indication that the hysteresis in the envelope of P in the experiment cannot be due uniquely to the viscoelastic change in reed properties.

Finally, fig. 8(a) also shows that a direct Hopf bifurcation takes place, since the RMS envelope approaches zero continuously as the blowing pressure decreases.

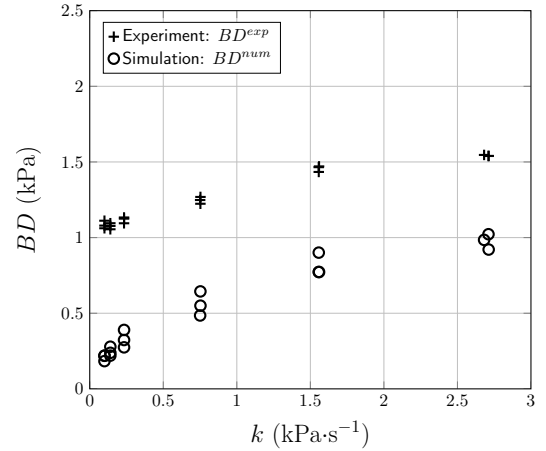


Figure 9: Bifurcation delay estimated on experimental signals (BD^{exp} (+)) and on simulated signals (BD^{num} (o)) as functions of the slope k .

4.3.2 Dynamic oscillation threshold

The indicators BD^{exp} and BD^{num} are plotted as functions of the slope k in fig. 9, where all recordings and all simulations are represented. The measurements are repeatable, showing little difference between the three tests of each slope k .

As suggested by fig. 8, the gaps BD^{exp} and BD^{num} are always positive and increase with the slope k . This is as predicted by recent theoretical predictions on a discrete time system affected with noise[24]. Figure 9 shows that the indicator BD^{num} estimated on numerical simulations is always smaller than the experimental BD^{exp} . A possi-

ble reason for this is that the static oscillation threshold is underestimated in the fit to the model (see sect. 4.1). Indeed, in fig. 8(b), the decreasing slope of simulations k_1 , k_2 and k_3 shows an extinction of the sound close to the static oscillation threshold $P_{mst} = 4.01\text{kPa}$. On the other hand, for experimental signals (cf. fig. 8(a)), the extinction is close to 4.5 kPa, which can indicate that the static threshold is close to this value. The consistently lower value of the estimated static oscillation threshold P_{mst} could in principle be due to an underestimation of the acoustic losses α . However, as pointed in section 3.1.1, using assumption (5), Dalmont and Frappe [5] obtain a good agreement between theoretical and experimental results. Therefore, we believe that the error in the static oscillation threshold probably comes from the estimation of the parameters P_M and ζ . Indeed, underestimation is common when using a fit of non-linear characteristics [25].

Despite this underestimation, the delay in the start of the oscillations still occurs even if the static threshold is close to 4.5 kPa. Moreover, its dependence on the variation of the parameter k is unchanged.

4.3.3 Growth constants of the onset transient

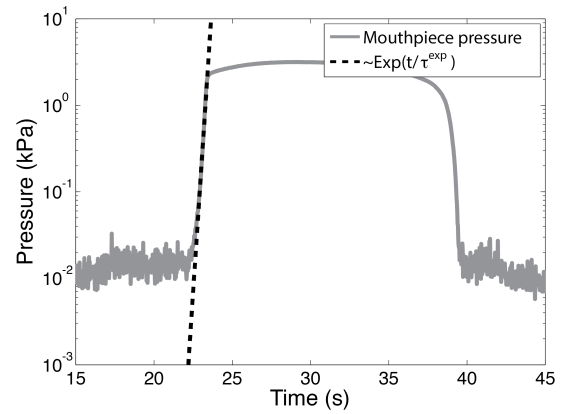
This section is devoted to comparing the indicators τ^{exp} , η^{exp} , τ^{num} and η^{num} .

First of all, fig. 10 shows an example of the mouthpiece pressure profile on a logarithmic scale (experimental signal in fig. 10(a) and simulated signal in fig. 10(b)) compared to the exponential fit of the onset transient (dashed line on fig. 10). Even if the mouth pressure depends on time (CIMP with $k = 0.23\text{kPa/s}$), the pressure P inside the mouthpiece (for both experimental and simulated signal) increases exponentially during the onset transient.

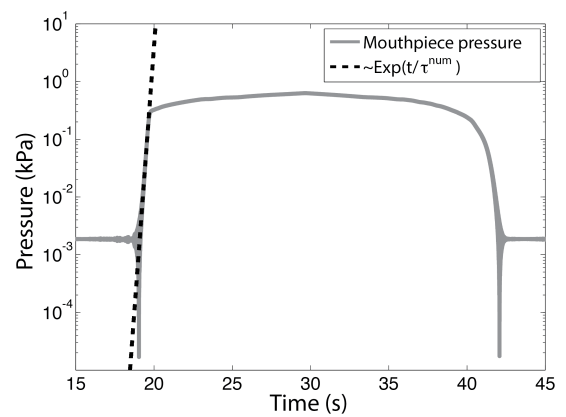
Figure 11 shows that τ^{exp} , η^{exp} , τ^{num} and η^{num} are close to each other. Figure 11(a) shows that τ^{exp} and τ^{num} decrease with the increase rate k of mouth pressure. Conversely, in fig. 11(b) η^{exp} and η^{num} appear to increase with k .

4.4 Discussion

The similarity between experimental and simulated envelope profiles (as functions of blowing pressure) provides a good indication that the simplistic model is able to provide good predictions of dynamic instrument behaviors, as it has already provided for static values of the parameters [5]. In different numerical simulations[10] of the same simple model the dynamic thresholds were found to be much higher than the ones found in experimental results, mostly because the time-profile of the pressure is not affected by noise whereas the experimental one is. A better prediction of the dynamic threshold can be performed by introducing stochastic variables in the modeling[24]



(a) Experiment



(b) Simulation

Figure 10: Time profile of the RMS envelope $P_{RMS}(t)$ (solid gray line) compared to its exponential fit during the onset transient (dashed black line). (a) Experimental signal and (b) simulated signal. $k = 0.23\text{kPa/s}$.

Secondly, the fact that the values P_{mdt}^{exp} (and also P_{mdt}^{num}) are always larger than the static oscillation threshold P_{mst} can be explained by the intrinsic difference between the system described by the static theory where the blowing pressure P_m is assumed to be constant (a *static* case) and the system used in experiments where the blowing pressure is increasing (a *dynamic* case). Recent theoretical and experimental works [11, 26, 27] on dynamic nonlinear systems show that, in dynamic cases (as in our experiments), the oscillations start significantly after the *static* theoretical threshold has been exceeded. This phenomenon is known as *bifurcation delay*.

Finally, the time growth constant τ decreases with the slope k of the blowing pressure. Conversely, the pressure growth constant η increases with k . This means that even if the speed (as a function of time) of the onset transient of the acoustic pressure inside the mouthpiece increases with k , the blowing pressure sees a smaller variation during the onset transient.

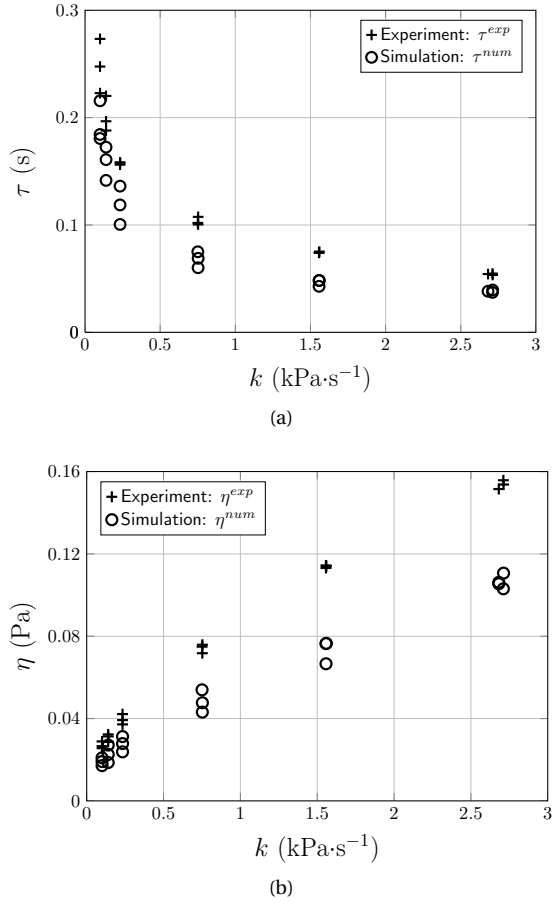


Figure 11: Parameters τ (a) and η (b) as a function of the increase rate k of blowing pressure. (+) Experiment and (o) simulation.

5. Results for the "IIMPP" profile

The aim of this section is to study the evolution of two indicators deduced from the mouthpiece pressure as a function of the increasing duration of the mouth pressure. The first indicator is the oscillation start time, compared to the “interrupting time” of the IIMPP. The second indicator is the time growing constant.

5.1 Indicator estimation

As in the previous section, a few indicators are extracted from the measured signals, although with a few differences. An illustration of the indicators is depicted in fig. 12.

The increasing phase of P_m is detected from a threshold on the derivative of the measured P_m . Two reference points, the start time $(t_{\text{start}})_{P_m}$ and the “interrupting time” $(t_{\text{end}})_{P_m}$, result from this detection, and allow to estimate the duration of the transient of the blowing pressure:

$$(\Delta t)_{P_m} = (t_{\text{end}})_{P_m} - (t_{\text{start}})_{P_m}. \quad (19)$$

Assuming that the growth of P_m is linear, its slope k is estimated between the times $(t_{\text{start}})_{P_m}$ and $(t_{\text{end}})_{P_m}$.

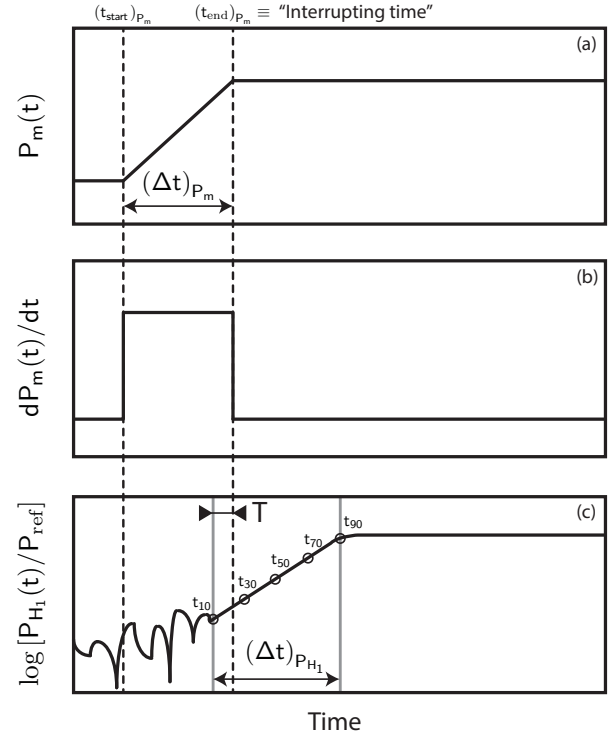


Figure 12: Schematic representation of (a) the blowing pressure P_m and (b) its first time derivative. (c) Schematic representation of $\log[P_{H_1}(t)]$. Gray lines depict the duration $(\Delta t)_{P_{H_1}}$ of the onset transient of the pressure P inside the mouthpiece. Vertical dashed lines demarcate the duration $(\Delta t)_{P_m}$ of the transient of P_m . The delay T , defined by equation (21), is also represented.

In this section, during the increasing part of the mouth pressure IIMPP profiles, the increase rates k are higher than the ones used in section 4. In this case, we have noted that the use of the amplitude of the first harmonic $P_{H_1}(t)$ instead of the RMS envelope $P_{RMS}(t)$ allows the detection of sound emergence at lower amplitudes.

Amplitude of individual harmonics is extracted using heterodyne detection. Detection of a component at frequency f is performed by constructing a new complex vector resulting from the product of signal x_n by $\exp(j2\pi ft)$. This vector is then multiplied by a 4-period-long window of type “Blackman-Harris”, and the absolute value of the result is summed over the window and normalized.

This algorithm was tested in 2 different signals: one with a jump in amplitude and one with a jump in frequency (from f to $2f$) with accurate results, and a precision (smoothing) of about 2 periods in both cases.

In fact, the noise background is lower if calculated at a narrower range of frequencies than for the RMS envelope which is wideband. Therefore, in this section transient parameters are estimated on $P_{H_1}(t)$.

Two reference values of $P_{H_1}(t)$ are first determined, a low one corresponding to the noise background close to the note end, and high value, the absolute maximum of the logarithm envelope. Then, the first value of $\log[P_{H_1}/P_{\text{ref}}]$ crossing the midpoint between these two

previous values is used as a reference time t_{50} . Four other points are detected with abscissa $\log[P_{H_1}/P_{\text{ref}}]$: t_{10} , t_{30} , t_{70} and t_{90} . Using these reference points the duration of the onset transient of the pressure P is defined as:

$$(\Delta t)_{P_{H_1}} = t_{90} - t_{10}. \quad (20)$$

Next, the delay T defines the difference in time between the beginning of the onset transient of P and the end of the blowing pressure increase:

$$T = t_{10} - (t_{\text{end}})_{P_m} \quad (21)$$

This indicator provides some information on the causality link between the discontinuity in the blowing pressure profile and the onset of oscillations, a positive value indicating that the oscillations may not be a consequence of the stop of the pressure growth.

Finally, assuming that the onset transient consists of an exponential growth where $P_{H_1}(t) \sim e^{t/\tau_{H_1}}$, the time growth constant τ_{H_1} is estimated as the slope of $\log[P_{H_1}(t)/P_{\text{ref}}]$ between t_{30} and t_{70} .

5.2 Experimental results

The indicators defined above are calculated for each trial. Some of the original trials were removed from the analysis when the fundamental frequency $f_0(t)$ was higher than expected ($\geq 200\text{Hz}$, whereas the expected playing frequency is around 160Hz) for a long period of time during the onset phase. These correspond to squeaks or higher regimes which afterwards decay to the fundamental. The trials where the onset phase lasts longer than 400ms were also removed. After this treatment, four signal are removed from the fifteen originals trials.

In the remainder of this paper, the figures show the averages of the indicators over 4 trials of a particular configuration (written with an overline) and the standard deviations as a function of the average of the measured $(\Delta t)_{P_m}$ noted $(\overline{\Delta t})_{P_m}$ (cf. table 2). Moreover, all time quantities are made dimensionless using $T_p = 1/f_p$, where $f_p \approx 160\text{Hz}$ is the playing frequency.

The example depicted in fig. 13 shows that the amplitude of the sound grows exponentially at the beginning of the onset. Moreover, we can see that the time growth constant τ_{H_1} looks constant regardless of the value of $(\Delta t)_{P_m}$.

Figure 14 shows the time growth constants τ_{H_1} obtained for each value of $(\Delta t)_{P_m}$. Figure 14 confirms the observations made in fig. 13: time growth constant τ_{H_1} does not depend on the value of $(\Delta t)_{P_m}$. The repeatability of the measurement is good for τ_{H_1} : the standard deviation is between 7% and 14% of the average.

Indicator T is plotted on fig. 15. We can notice that the beginning of the onset transient of the mouthpiece pressure is close to the ‘‘interrupting time’’ of the blowing pressure.

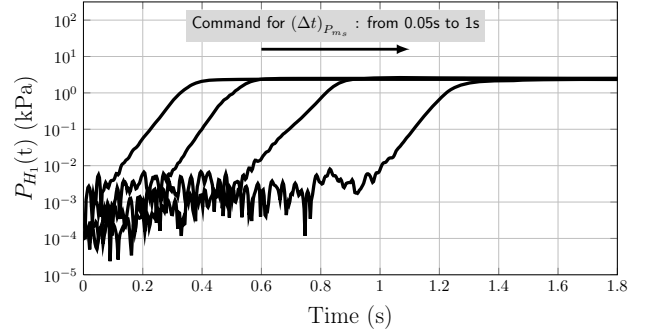


Figure 13: Example of the time evolution $P_{H_1}(t)$ for each value of $(\Delta t)_{P_m}$. A logarithmic scale is used for the ordinate axis.

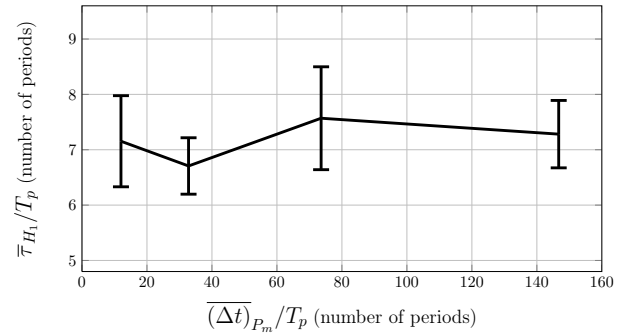


Figure 14: Average and standard deviation (error bars) of the time growth constant τ_{H_1} obtained for each value of $(\overline{\Delta t})_{P_m}$.

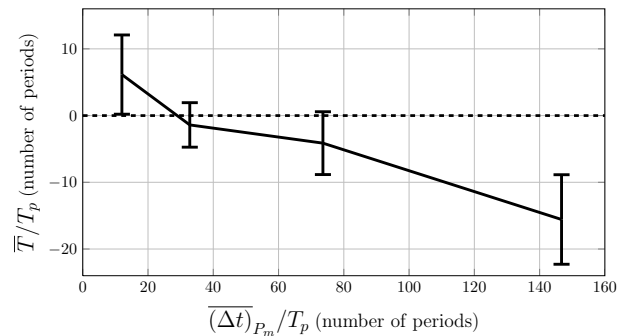


Figure 15: Average plus or minus the standard deviation of the duration T obtained for each value of $(\Delta t)_{P_m}$.

5.3 Discussion

In a fast linear increase in the blowing pressure followed by a stationary phase (i.e. IIMPP case), the results highlight that there is no “soft or fast” onset when the tongue is not used. The speed (i.e. τ_{H_1}) of the onset transient of sound is roughly the same regardless of the duration of the blowing pressure transient. The only impact of increasing $(\Delta t)_{P_m}$ is an increased delay in the curve of P_{H_1} (cf. fig. 13). Silva *et al.* [12] obtained similar conclusions on numerical simulations.

A possible reason for this is the fact that the beginning of the onset transient of the mouthpiece pressure is close to the end of the blowing pressure growth. This is shown in fig. 15 where the variable T is plotted. Therefore, for most of the mouthpiece pressure onset transient, the mouth pressure is constant and equal for each experiment, i.e. oscillations increase in “static” situation. In this case, as recalled in section 3.3, simple linear loop models predict that the time growth constant depends only on the value of the constant mouth pressure. However, to conclude that for IIMPP profiles the time growth constant of the mouthpiece pressure in the onset transient depends only on the target value of the mouth pressure, further measurements with different target values of the mouth pressure are required.

The influence of the increase rate k on the time growth constant τ^{exp} seen in section 4 could be explained by the fact that blowing pressure still increases during the onset transient.

6. Conclusion

When a clarinet is blown using a linearly increasing mouth pressure, oscillations appear at a much higher value than those predicted by static bifurcation theory. This explains why increasing sweeps of the blowing pressure do not provide accurate information on the oscillation close to the static oscillation threshold. Decreasing the rate of pressure variation shows a limited improvement.

For interrupted fast attacks in mouth pressure, the oscillations start at the moment the blowing pressure is stabilized. The oscillations then follow an exponential envelope with a time growth constant that only depends on the target values of the parameters. An extension to musical contexts would require a validation with in vivo measurements taking into account more complex mouth pressure profiles and the influence of the tongue.

Finally, the similarity observed between experimental and simulated envelope profiles suggests that the complex behaviors observed experimentally with a time-varying blowing pressure can be described analytically by applying the same blowing pressure time profile to a simple classical model of the clarinet.

Acknowledgments

The authors thank Mrs Marilyn Twell for proofreading.

This work is financed by the research project SDNS-AIMV “Systèmes Dynamiques Non-Stationnaires - Application aux Instruments à Vent” financed by *Agence Nationale de la Recherche*.

Appendices

A. Explicit expression of the function G

The analytical expression for function G , defined by equation (9), is obtained by Taillard *et al* [3]. Its expression is recalled in this appendix where the following notations are used:

$$P = P^+ + P^- = G(x) - x; \quad (22)$$

$$U = P^+ - P^- = \frac{1}{Z_c} (G(x) + x). \quad (23)$$

These notations are slightly different from those used by Taillard *et al* [3].

From the expression of the nonlinear characteristic, given by equations (1), the non-beating regimes with positive flow and negative flow can be explicitly written:

$$\left\{ \begin{array}{l} U(\Delta P) = \frac{\zeta}{Z_c} (P_M - \Delta P) \sqrt{\frac{\Delta P}{P_M}} \quad (24a) \\ \text{if } 0 < \Delta P < P_M \text{ (Non-beating reed, positive flow);} \\ U(\Delta P) = -\frac{\zeta}{Z_c} (P_M - \Delta P) \sqrt{\frac{-\Delta P}{P_M}} \quad (24b) \\ \text{if } -P_M < \Delta P < 0 \text{ (Non-beating reed, negative flow);} \\ U(\Delta P) = 0 \quad (24c) \\ \text{if } \Delta P > P_M \text{ (Beating reed).} \end{array} \right.$$

In the following sections, we recall the analytical expression for function G for each of the three operating regimes (beating regime, non-beating regime with positive flow and negative flow) of the instrument.

A.1 Beating reed regime

For the beating case, the flow U is equal to zero. Therefore, from equation (23), the expression of G is simply:

$$G(x) = -x. \quad (25)$$

A.2 Non-beating reed regimes

From equation (22) and recalling that $\Delta P = P_m - P$, function G can be written as follow:

$$G(x) = P_m + \Delta P(U) + x. \quad (26)$$

Therefore, inverting equations (24b) and (24c) leads to a direct analytical expression of function G for the positive and negative flow cases respectively. In practice, inverting (24b) and (24c) consists in solving a third order polynomial equation, as explained by Taillard *et al* [3].

A.2.1 Positive flow

For the non-beating reed regime with positive flow, the analytical expression for function G is:

$$G(x) = P_m - P_M \left(-\frac{2}{3} \eta \sin \left(\frac{1}{3} \arcsin \left(\frac{\psi - \frac{9}{2} \left(\frac{3}{P_M} (P_m + 2x) - 1 \right)}{\zeta \eta^3} \right) \right) + \frac{1}{3\zeta} \right)^2 + x, \quad (27)$$

with,

$$\psi = \frac{1}{\zeta^2} \quad ; \quad \eta = \sqrt{3 + \psi}. \quad (28)$$

A.2.2 Negative flow

As stated above, inverting equation (24c) consists in solving a third order polynomial equation. For the non-beating reed regime with negative flow, the analytical expression of function G depends on the sign of the discriminant of the polynomial:

$$\text{Discr} = q^3 + r^2, \quad (29)$$

with

$$q = \frac{1}{9} (3 - \psi) \quad ; \quad r = -\frac{\psi + \frac{9}{2} \left(\frac{3}{P_M} (P_m + 2x) - 1 \right)}{27\zeta}. \quad (30)$$

Positive discriminant. In this case, the expression of G is:

$$G(x) = P_m + P_M \left(s_1 - \frac{q}{s_1} - \frac{1}{3\zeta} \right)^2 + x, \quad (31)$$

where,

$$s_1 = \left[r + \sqrt{\text{Discr}} \right]^{1/3}. \quad (32)$$

Negative discriminant. G is:

$$G(x) = P_m +$$

$$P_M \left(\frac{2}{3} \eta' \cos \left(\frac{1}{3} \arccos \left(\frac{-\psi - \frac{9}{2} \left(\frac{3}{P_M} (P_m + 2x) - 1 \right)}{\zeta \eta'^3} \right) \right) - \frac{1}{3\zeta} \right)^2 + x, \quad (33)$$

with,

$$\eta' = \sqrt{-3 + \psi}. \quad (34)$$

References

- [1] V. Debut and J. Kergomard, "Analysis of the self-sustained oscillations of a clarinet as a van der pol oscillator", in *18th International Congress on Acoustics-ICA*, volume 2, 1425–1428 (2004).
- [2] J. P. Dalmont, J. Gilbert, J. Kergomard, and S. Ollivier, "An analytical prediction of the oscillation and extinction thresholds of a clarinet", *J. Acoust. Soc. Am.* **118**, 3294–3305 (2005).
- [3] P. Taillard, J. Kergomard, and F. Laloë, "Iterated maps for clarinet-like systems", *Nonlinear Dynam.* **62**, 253–271 (2010).
- [4] J. Kergomard, S. Ollivier, and J. Gilbert, "Calculation of the spectrum of self-sustained oscillators using a variable truncation method", *Acta. Acust. Acust.* **86**, 665–703 (2000).
- [5] J. P. Dalmont and C. Frappe, "Oscillation and extinction thresholds of the clarinet: Comparison of analytical results and experiments", *J. Acoust. Soc. Am.* **122**, 1173–1179 (2007).
- [6] A. Chaigne and J. Kergomard, "Instruments à anche (reed instruments)", in *Acoustique des instruments de musique (Acoustics of musical instruments)*, chapter 9, 400–468 (Belin) (2008).
- [7] S. Karkar, C. Vergez, and B. Cochelin, "Oscillation threshold of a clarinet model: A numerical continuation approach", *The Journal of the Acoustical Society of America* **131**, 698–707 (2012).
- [8] B. Gazengel and J. P. Dalmont, "Mechanical response characterization of saxophone reeds", in *6th Forum Acusticum* (Aalborg, Denmark, 26 June-1 July 2011).
- [9] M. Atig, J. P. Dalmont, and J. Gilbert, "Saturation mechanism in clarinet-like instruments, the effect of the localised nonlinear losses", *Appl. Acoust.* **65**, 1133–1154 (2004).

- [10] B. Bergeot, C. Vergez, A. Almeida, and B. Gazengel, "Prediction of the dynamic oscillation threshold in a clarinet model with a linearly increasing blowing pressure", *Nonlinear Dynam.* **73**, 521–534 (2013), URL <http://dx.doi.org/10.1007/s11071-013-0806-y> (date last viewed 5/28/13).
- [11] A. Fruchard and R. Schäfke, "Sur le retard à la bifurcation (on the bifurcation delay)", *Arima* **9**, 431–468 (2008).
- [12] F. Silva, P. Guillemain, J. Kergomard, C. Vergez, and V. Debut, "Some simulations of the effect of varying excitation parameters on the transients of reed instruments", (2013-01), URL <http://hal.archives-ouvertes.fr/hal-00779636> (date last viewed 5/28/13).
- [13] D. Ferrand and C. Vergez, "Blowing machine for wind musical instrument : toward a real-time control of blowing pressure", in *16th IEEE Mediterranean Conference on Control and Automation (MED)*, 1562–1567 (Ajaccion, France) (2008).
- [14] D. Ferrand, C. Vergez, B. Fabre, and F. Blanc, "High-precision regulation of a pressure controlled artificial mouth : the case of recorder-like musical instruments", *Acta. Acust. Acust.* **96**, 701–712 (2010).
- [15] C. J. Nederveen, *Acoustical aspects of woodwind instruments* (Northern Illinois University Press, Illinois) 28–35 (Revised edition, 1998).
- [16] D. H. Keefe, "Acoustical wave propagation in cylindrical ducts: transmission line parameter approximations for isothermal and non-isothermal boundary conditions", *J. Acoust. Soc. Am.* **75**, 58–62 (1984).
- [17] C. Maganza, R. Caussé, and F. Laloë, "Bifurcations, period doublings and chaos in clarinet-like systems", *EPL (Europhysics Letters)* **1**, 295 (1986).
- [18] J. Kergomard, "Elementary considerations on reed-instrument oscillations", in *Mechanics of musical instruments by A. Hirschberg/ J. Kergomard/ G. Weinreich*, volume 335 of *CISM Courses and lectures*, chapter 6, 229–290 (Springer-Verlag) (1995).
- [19] J. Kergomard, J. P. Dalmont, J. Gilbert, and P. Guillemain, "Period doubling on cylindrical reed instruments", in *Proceeding of the Joint congress CFA/DAGA 04*, 113–114 (Société Française d'Acoustique - Deutsche Gesellschaft für Akustik) (2004, Strasbourg, France).
- [20] S. Ollivier, J. P. Dalmont, and J. Kergomard, "Idealized models of reed woodwinds. part 2 : On the stability of two-step oscillations", *Acta. Acust. united Ac.* **91**, 166–179 (2005).
- [21] J. P. Dalmont, J. Gilbert, and S. Ollivier, "Nonlinear characteristics of single-reed instruments: Quasi-static volume flow and reed opening measurements", *J. Acoust. Soc. Am.* **114**, 2253–2262 (2003).
- [22] A. Almeida, C. Vergez, and R. Caussé, "Quasi-static nonlinear characteristics of double-reed instruments", *J. Acoust. Soc. Am.* **121**, 536–546 (2007).
- [23] K. Jensen, "Enveloppe model of isolated musical sounds", *Proceedings of the 2nd COST G-6 Workshop on Digital Audio Effects (DAFx99)*, NTNU, Trondheim (1999).
- [24] B. Bergeot, C. Vergez, A. Almeida, and B. Gazengel, "Prediction of the dynamic oscillation threshold in a clarinet model with a linearly increasing blowing pressure: Influence of noise", *Nonlinear Dynam.* **74**, 591–605 (2013), URL <http://dx.doi.org/10.1007/s11071-013-0991-8> (date last viewed 10/17/13).
- [25] D. Ferrand, C. Vergez, and F. Silva, "Seuils d'oscillation de la clarinette : validité de la représentation excitateur-résonateur (oscillation thresholds of the clarinet: validity of the resonator-exciter representation)", in *10ème Congrès Français d'Acoustique* (Lyon, France, April 12nd-16th 2010).
- [26] A. Fruchard and R. Schäfke, "Bifurcation delay and difference equations", *Nonlinearity* **16**, 2199–2220 (2003).
- [27] J. R. Tredicce, G. Lippi, P. Mandel, B. Charasse, A. Chevalier, and B. Picqué, "Critical slowing down at a bifurcation", *Am. J. Phys.* **72**, 799–809 (2004).